Report

www.the-innovation.org

Realizing the thinnest hydrodynamic cloak in porous medium flow

Mengyao Chen,[1] Xiangying Shen,[1,2,*] and Lei Xu[1,*]

*Correspondence: shenxy@sustech.edu.cn (X.S.); xuleixu@cuhk.edu.hk (L.X.)

Received: March 23, 2022; Accepted: May 19, 2022; Published Online: May 25, 2022; https://doi.org/10.1016/j.xinn.2022.100263

GRAPHICAL ABSTRACT

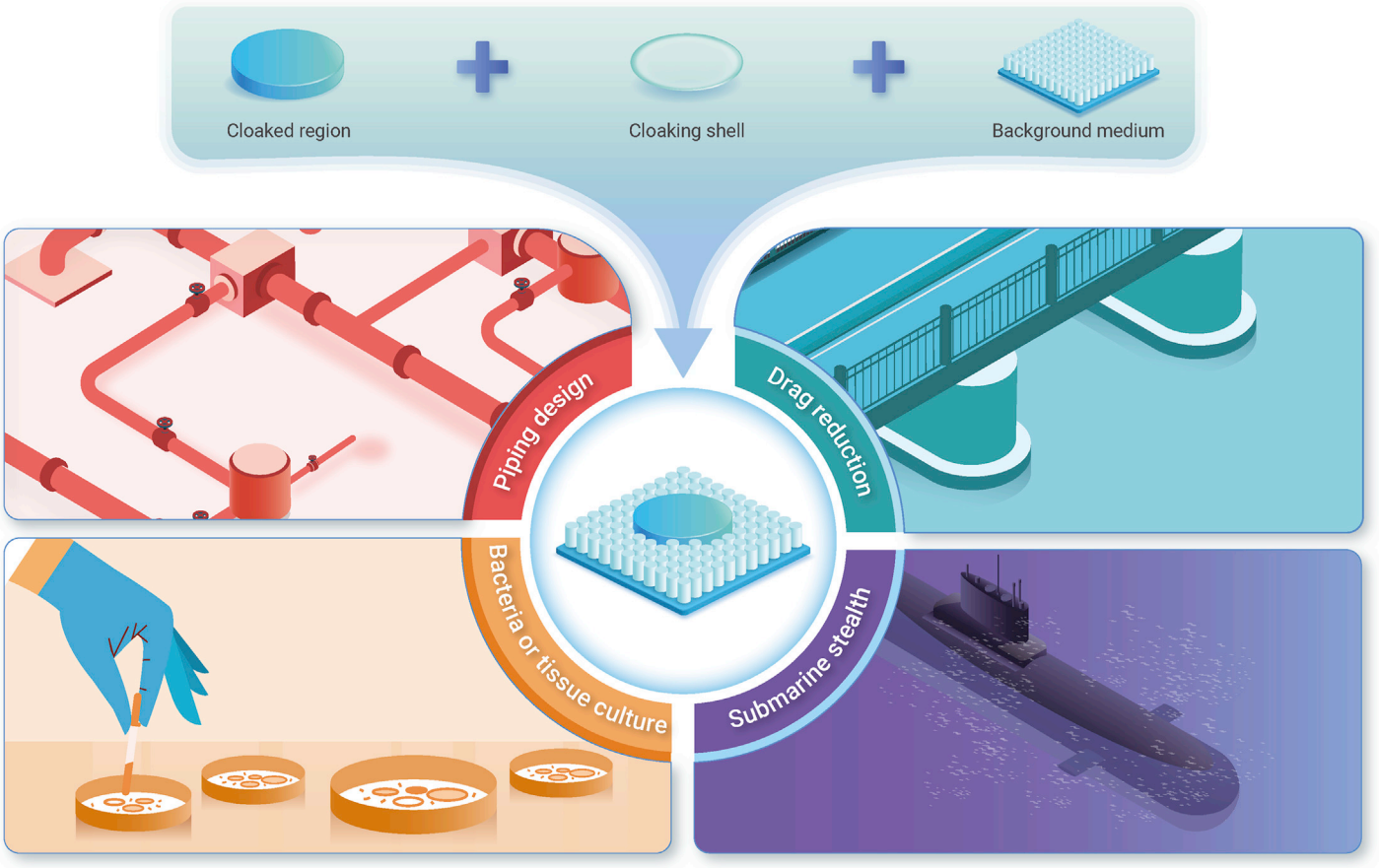

PUBLIC SUMMARY

- A hydrodynamic cloak has been experimentally realized in a porous medium flow field
- It is the thinnest shell-shaped cloak ever designed. The cloak structure is unparallelly simple
- The cloak structure is unparallelly simple. It consists of a thin shell of free space and an isotropic porous medium

Report

Realizing the thinnest hydrodynamic cloak in porous medium flow

Mengyao Chen,[1] Xiangying Shen,[1,2,*] and Lei Xu[1,*]

[1]The Department of Physics, The Chinese University of Hong Kong, Shatin, Hong Kong, China

[2]The Department of Materials Science and Engineering, Southern University of Science and Technology, Shenzhen 518055, China

*Correspondence: shenxy@sustech.edu.cn (X.S.); xuleixu@cuhk.edu.hk (L.X.)

Received: March 23, 2022; Accepted: May 19, 2022; Published Online: May 25, 2022; https://doi.org/10.1016/j.xinn.2022.100263

Citation: Chen M., Shen X., and Xu L. (2022). Realizing the thinnest hydrodynamic cloak in porous medium flow. The Innovation **3(4)**, 100263.

Transformation mapping theory offers us great versatility to design invisible cloaks for the physical fields whose propagation equations remain invariant under coordinate transformations. Such cloaks are typically designed as a multi-layer shell with anisotropic material properties, which makes no disturbance to the external field. As a result, an observer outside the cloak cannot detect the existence of this object from the field disturbances, leading to the invisible effect in terms of field prorogation. In fact, for many prorogating fields, at a large enough distance, the field distortion caused by an object is negligible anyway; thus, a thin cloak is desirable to achieve near-field invisibility. However, a thin cloak typically requires more challenging material properties, which are difficult to realize due to the huge variation of anisotropic material parameters in a thin cloak region. For a flow field in a porous medium, by applying the bilayer cloak design method and integrating the inner layer with the obstacle, we successfully reduce the anisotropic multi-layer cloak into an isotropic single-layer cloak. By properly tailoring the permeability of the porous medium, we realize the challenging material parameters required by the ultrathin cloak and build the thinnest shell-shaped cloak of all physical fields up to now. The ratio between the cloak's thickness and its shielding region is only 0.003. The design of such an ultrathin cloak may help to achieve the near-field invisibility and concealment of objects inside a fluid environment more effectively.

INTRODUCTION

Making an object invisible has always been a dream for many scientists and engineers. Thanks to pioneering theoretical studies,[1–3] transformation mapping theory shows great potential for the design of invisible cloaks in various physical fields. The transformation mapping theory predicts that once the governing equation of a transport process remains form invariant under a certain coordinate transformation, one can tailor the medium's transport parameters with the coordinate transformation to achieve a desirable propagation of the corresponding physical field. With this theory, researchers may design cloaks that can shield its inner space from external detection and make inside objects invisible in various situations, such as optics,[4,5] magnetics,[6,7] acoustics,[8,9] heat transfer,[10–12] and even time.[13,14] In hydrodynamics, similarly invisible cloaks have also been proposed to conceal the objects without disturbing the surrounding fluid field and are useful for target stealth and drag reduction.[15–17] Although different structures have been experimentally[16,17] and theoretically[18–20] studied, the thickness of the cloak has never been systematically tuned. However, thickness is a key factor for cloaking performance, because, at a large distance, the disturbance from the object is typically negligible anyway, and a cloak with a large thickness is thus meaningless in practice. Therefore, it is desirable to design cloaks as thin as possible. In this study, we successfully achieve an ultrathin cloak, whose dimensionless thickness (i.e., the cloak thickness divided by the shielded region's size) is thinner than all previous cloaks practically realized.

The conventional design of a cloak based on the transformation mapping theory is to form multiple layers with anisotropic materials, which naturally results in a large cloak thickness. Hence, a new design with fewer layers is desirable to reduce the thickness. When the dominant transport equation is the Laplace equation,[6,11,21] cloaks can be designed as bilayer structures with isotropic materials, which can achieve a much thinner thickness. In an electromagnetic field, the bilayer cloak has achieved a dimensionless thickness of $\sigma = 0.25$.[22] In a direct current (DC) electric field, σ of an electric bilayer cloak is about 0.17.[23] In thermodynamics, researchers started to pursue the ultrathin cloak for the first time and reduced this ratio to an amazing value of 0.02.[24] In this study, we further decrease σ by another order of magnitude and reach the striking value of 0.003 in the flow field inside a porous medium.

In porous medium hydrodynamics, due to the low Reynolds number, the Navier-Stokes equation can be simplified into Darcy's law, which is in the form of the Laplace equation. Therefore, bilayer cloaks can be designed with homogeneous and isotropic materials, which offers a good opportunity to realize an ultrathin cloak.

Inside a porous medium, permeability is the dominant control parameter that controls transport properties, which can be determined entirely by the artificially constructed porous structure. By placing small pillars in desired locations and tuning their sizes and spacings (i.e., tuning the porosity of the medium), the permeability can be tailored accurately. In addition, due to the sensitive permeability-porosity relationship, by only slightly changing porosity, the permeability can be adjusted broadly over several orders of magnitude. As a result, this accurate and broad tuning enables an ultrathin cloak with $\sigma = 0.003$, the thinnest cloak ever achieved experimentally.

THEORETICAL DESIGN

In general, the cloaking or invisible effect can be achieved by establishing a perfect impedance match between the background and the cloaking shell. The spatial distribution of the transmission parameters in the cloaking shell needs to make the streamlines bypass the shielded object. In previous studies, owing to the sophisticated and anisotropic parameters distributed in the cloaking shell, the overall thickness of cloaks is typically quite large. However, for a flow field inside a porous medium, we now demonstrate an ultrathin cloak design.

Our ultrathin cloak is based on the bilayer cloak design method instead of the transformation mapping theory. In principle, the bilayer method is suitable for the fields governed by the Laplace equation. It consists of an inner isotropic layer with a near-zero material parameter (such as the permeability in our case) and an outer isotropic layer whose parameter is derived from solving the Laplace equation. This bilayer method is mature and has been applied to design cloaks in various propagating fields, such as the magnetic field,[25] thermal conduction,[11] DC current,[25] and particle diffusion systems.[26] To reduce the thickness even further, we use the outer wall of the hidden object as the inner layer of the bilayer cloak due to its zero permeability and realize a single-layer design demonstrated below.

We consider a two-dimensional (2D) flow inside a porous medium, with a small Reynolds number to satisfy a laminar flow: $Re = \rho_0 u_0 R/\mu_0 \ll 1$, where ρ_0 and μ_0 are the fluid's density and dynamic viscosity respectively, u_0 is the uniform background velocity, and R is a characteristic linear dimension (in our case it is the thickness of cloak). The pressure difference between the high-pressure region with $p = p_H$ to the low-pressure region with $p = p_L$ produces a uniform background flow with velocity u_0. Under these conditions, the Navier-Stokes equation is reduced to the Brinkman-Stokes equation

$$\mu \nabla^2 \vec{u} = \vec{\nabla} p + \mu_0 k^{-1} \vec{u} \qquad \text{(Equation 1)}$$

where μ is the effective viscosity of the flow in the porous medium,[27,28] k is the permeability, and p is pressure. In the limit of the small permeability $k \ll R_1^2$, the term $\mu \nabla^2 \vec{u}$ is much smaller than $\mu_0 k^{-1} \vec{u}$ and thus is negligible. Then the Brinkman-Stokes equation is simplified into Darcy's law:

$$\vec{\nabla} p = \mu_0 k^{-1} \vec{u} \qquad \text{(Equation 2)}$$

The velocity field $\vec{u}$ is divergence free and the continuity equation for an incompressible fluid is:

$$\vec{\nabla} \cdot \vec{u} = 0 \qquad \text{(Equation 3)}$$

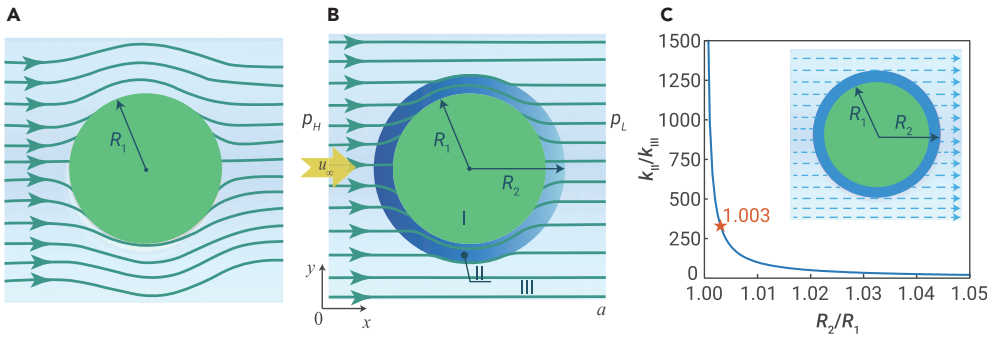

Figure 1. Schematic of the designed cloak in the porous medium domain (A) An impermeable obstacle ($r = R_1$) in the steady flow and streamlines in the background are distorted. (B) The obstacle with the cloaking shell ($R_1 < r < R_2$) (marked as the purple circular shell), and streamlines in the background remain parallel and uniform. (C) The curve represents the ratio of permeability in the background and the cloaking shell k_{II}/k_{III} versus the thickness ratio R_2/R_1. The orange star indicates the value of the cloak realized in our experiments. The inset is the cloak with uniform pressure contours, denoted as black dashed lines.

By substituting Equation 2 into Equation 3, the Darcy law can be transformed into the form of the Laplace equation:

$$\nabla \cdot (k\vec{\nabla}p) = 0 \qquad \text{(Equation 4)}$$

With this Laplace equation, we can build a 2D model of a cloak in porous medium. A cylindrical obstacle with the radius of R_1 is placed in the middle of the flow field as illustrated in Figure 1A. A cloaking shell is designed to wrap the obstacle and prevents it from disturbing the external flow field, making it invisible with respect to the external flow. As demonstrated in Figure 1B, the entire space is divided into three regions: I, the impermeable obstacle ($0 < r < R_1$); II, the cloaking shell ($R_1 < r < R_2$); and III, the background ($r > R_2$). By solving the Laplace equation (Equation 4) in each region, we obtain its analytical solution expressed as:

$$p_i = A_0^i + B_0^i \ln r + \sum_{m=0}^{\infty}\left[A_m^i \sin(m\theta) + B_m^i \cos(m\theta)\right] r^m + \sum_{m=0}^{\infty}\left[C_m^i \sin(m\theta) + D_m^i \cos(m\theta)\right] r^{-m} \qquad \text{(Equation 5)}$$

Here, i = I, II, III denotes the different regions; A_0^i, B_0^i, A_m^i, B_m^i, C_m^i, and D_m^i are corresponding coefficients whose values can be obtained with the boundary conditions; and (r, θ) refers to the spatial position in the polar coordinate system. With boundary conditions and non-singular requirement in each region, we can derive that $m = 1$ and $A_1^i = C_1^i = B_0^i = 0$. Thus p_i is reduced into:

$$p_i = A_0^i + B_1^i r\cos\theta + D_1^i r^{-1}\cos\theta \qquad \text{(Equation 6)}$$

where p_i denotes the pressure in region i.

Applying the boundary conditions that the pressure and velocity are continuous at the interfaces of different regions and the normal velocity is zero at the surface of the impermeable obstacle (i.e., $k_I = 0$):

$$\begin{cases} p_{III}|_{r=R_2} = p_{II}|_{r=R_2} \\ p_{II}|_{r=R_2} = p_I|_{r=R_1} \\ k_{III}\dfrac{\partial p}{\partial r}\Big|_{r=R_2} = k_{II}\dfrac{\partial p}{\partial r}\Big|_{r=R_2} \\ k_{II}\dfrac{\partial p}{\partial r}\Big|_{r=R_1} = k_I\dfrac{\partial p}{\partial r}\Big|_{r=R_1} = 0 \end{cases} \qquad \text{(Equation 7)}$$

Substituting the above equation into Equation 6, and taking into account that p_{III} is equal to $(p_H - p_L)r\cos\theta$, we obtain the analytic expression for our 2D cloak as:

$$\frac{k_{II}}{k_{III}} = \frac{R_2^2 + R_1^2}{R_2^2 - R_1^2} = \frac{(R_2/R_1)^2 + 1}{(R_2/R_1)^2 - 1} \qquad \text{(Equation 8)}$$

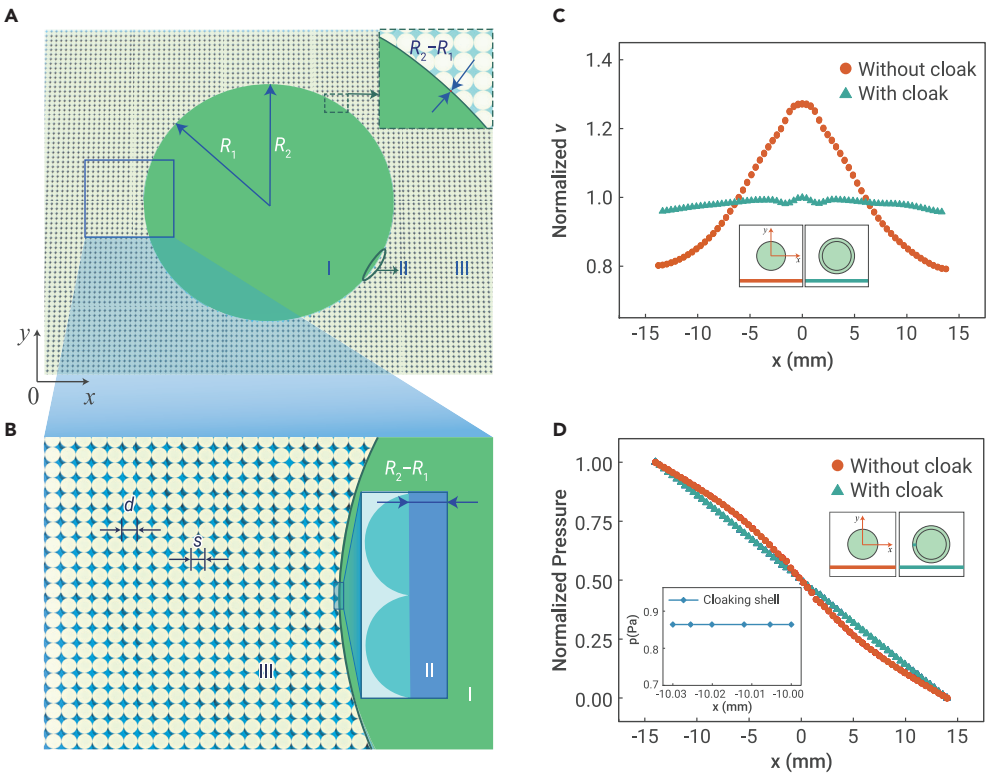

Figure 2. The ultrathin cloak realized by the porous medium (A) The structure of the ultrathin cloak composed of a shell of free space and the background medium of isotropic pillars. (B) Detailed view of the cloak structure, in which the yellow color represents the free-space shell (region II) with the thickness of $R_2 - R_1$. (C) Plot of the normalized numerical velocity changing with x in the case of cloak and only obstacle. All the numerical velocities in the two cases are normalized by the velocity at $x = 0$ in the case of cloak, and x is the position of the velocity. The inset shows the observation lines in the two cases. (D) The pressure distribution at the observation lines. The inset about the pressure curve indicates the zero-pressure gradient in the cloaking shell. The positions of observation lines in the two cases are shown in the inset at the top right.

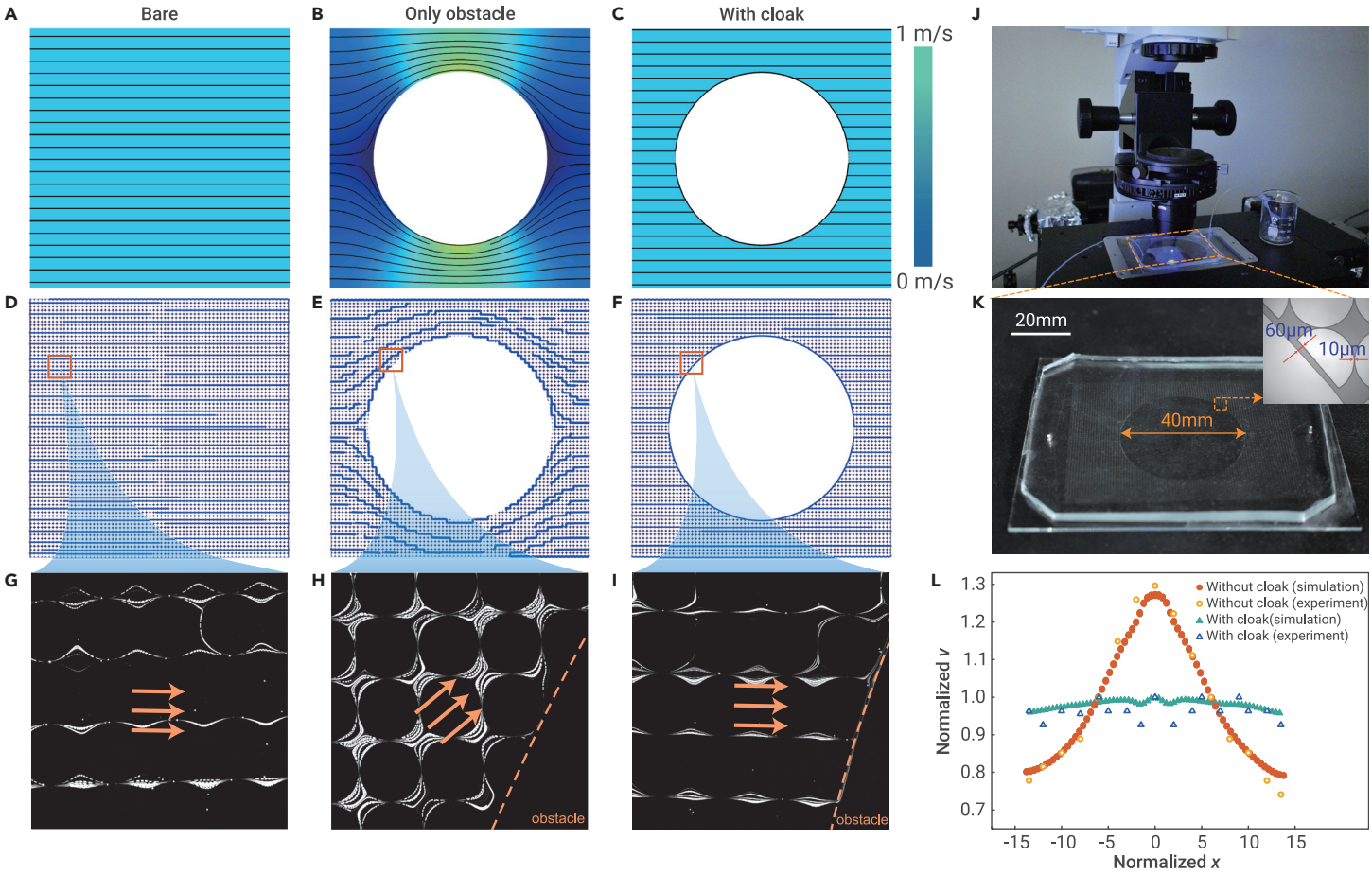

Figure 3. Numerical and experimental validation of the ultrathin cloak in hydrodynamics (A–C) Parametric simulations of velocity fields with the required permeability in the bare case (A), only obstacle (B), and the cloak (C). (D–F) Simulated velocity field in the bare case (D), only obstacle (E), and the cloak (F)with the porous medium of isotropic pillars. (G–I) The experimentally captured streamlines in the porous medium for the bare case (G), only obstacle (H), and the cloak case (I). (J) The fluorescence microscopy setup. (K) The PDMS microfluidic device, and the inset shows the thickness of the free-space shell of 60 μm and the pillar-to-pillar spacing of 10 μm. (L) Comparison of the velocity between experiment and simulation. The velocities in simulation are normalized by the numerical value at $x = 0$ in the case of cloak, and the velocity in experiment is normalized by the experimental value at $x = 0$ in the case of cloak. The device in the experiment is scaled down twice so that the simulation and experiment data can be collapsed in the same plot.

The above cloak solution can be understood from the following physical interpretation. An obstacle in the flow field is impermeable to fluid, and its permeability is thus zero. According to Darcy's law, streamlines will always bypass a region with zero permeability. In other words, the obstacle "repels" the streamlines and an external observer will observe this distortion of the flow field and detect the obstacle's existence. To achieve invisibility, a region with a permeability higher than the background that "attracts" the streamlines is required that can cancel out the repelling effect of the obstacle. Referring to Equation 8, the cloaking shell of region II is such a region with a higher permeability than the background (i.e., $k_{II} > k_{III}$). A proper geometric relationship between the cloaking shell and the obstacle will cancel the distortion of the flow field and yield a perfect cloaking or invisible effect.

Equation 8 represents an exact relation between permeability k_{II}, k_{III}, and the dimensionless ratio $R_2/R_1 = \sigma + 1$, where $\sigma = (R_2 - R_1)/R_1$ is the dimensionless cloak thickness. The dependence is shown in Figure 1C: k_{II}/k_{III} dramatically increases as R_2/R_1 approaches 1 or σ approaches 0, indicating that an ultrathin cloaking shell requires an extremely large k_{II}/k_{III}. However, this challenging requirement can be satisfied in a porous medium as shown below.

In order to form the porous medium, we place pillars uniformly in the background region, and, by controlling the distance between pillars, its permeability can be tailored. Based on the effective medium approximation, at a scale much larger than pillar distance, such a porous medium can be regarded as homogeneous and isotropic with a constant effective permeability. For a hydrodynamic flow, the permeability k and the porosity ϵ follow the power law of $k \sim \epsilon^3$ [29] for square arrays of identical pillars, and the porosity ϵ is defined as $\epsilon = 4s^2/\pi d^2$, in which d is the diameter of pillars and s is the center-to-center spacing between two neighboring pillars, as shown in Figures 2A and 2B. For a fixed diameter d, we can obtain the scaling $k \sim s^6$. Clearly, k is extremely sensitive to distance s, and a wide range of permeability can be achieved by simply changing the distance s for pillars with a fixed diameter.

Therefore, we can realize an ultrathin single-layer cloak with an unprecedented thickness: the cloaking shell is a thin layer of free space with an almost negligible thickness relative to the obstacle size, 0.3%. Here, free space means a thin layer of space without pillars. It may seem that, if there is no pillar, the free space is not a porous medium and its permeability is not well defined. However, due to the thin cloaking shell and the boundary influence from the surrounding porous medium, there is an effective permeability in this thin cloaking shell, as calculated later. Thus, our cloak is designed as an ultrathin layer of free space that encloses the solid obstacle and forms the region II ($(R_1 < r < R_2)$), which has an effective permeability k_{II}, and the pillars outside form the background region III ($(r > R_2)$) with isotropic permeability k_{III}, as depicted in Figures 2A and 2B.

As a specific demonstration of how to design the system, we fix the radius of the center obstacle at $R_1 = 10$ mm, the diameter of pillars at $d = 400$ μm, and the thickness of the free-space shell at $R_2 - R_1 = 30$ μm, which is only 0.3% of the obstacle radius $R_1 = 10$ mm, and numerically change the pillar spacing s as the only control parameter. According to Equation 8, we obtain $k_{II}/k_{III} \approx 334$, which is quite large and could be difficult to achieve in other material properties. However, with the power-law relationship of the sixth power $k \sim s^6$ in a porous medium, the permeability k_{III} varies dramatically even with a slight change in spacing s. With the numerical simulations of COMSOL Multiphysics, we find the optimized spacing at $s = 405$ μm, which achieves the best cloaking or invisibility effect. For comparison, the velocity and the pressure variations with and without a cloak are shown in Figures 2C and 2D, respectively. Without a cloak, the magnitude of velocity near the obstacle varies significantly,

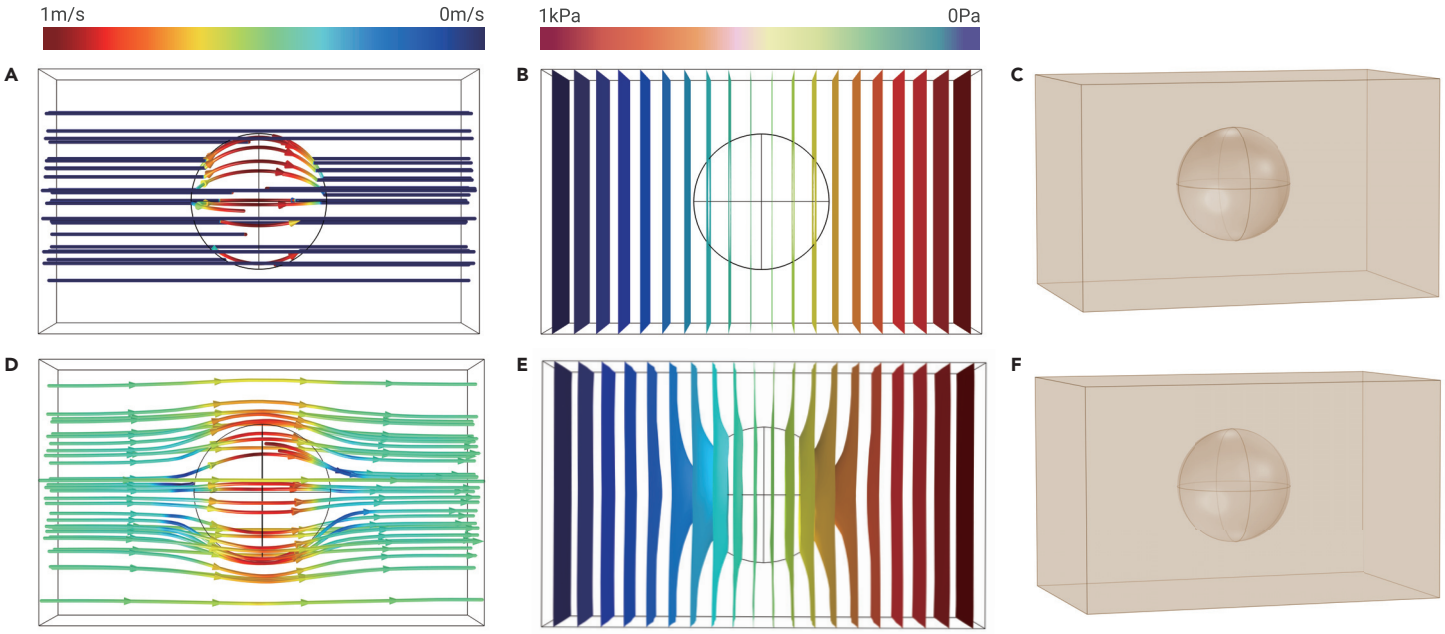

Figure 4. The numerical simulations of the 3D ultrathin hydrodynamic cloak (here R_1 = 1 mm and R_2 = 1.003 mm) (A–F) The streamlines (A) and the iso-pressure surface (B) are straight with the 3D cloak, while they are significantly distorted near the object without the 3D cloak in (D) and (E). The 3D images with and without the 3D ultrathin cloak are shown in (C) and (F). Since the thickness of the cloak is only 0.3% of the cloaked object, the size difference between (C) and (F) cannot be distinguished by the naked eye.

while it remains quite stable with a cloak. The pressure variation also becomes linear with a cloak, indicating a constant pressure gradient undisturbed by the obstacle. Therefore, our ultrathin cloak achieves the invisibility function successfully and an external observer cannot observe the flow field distortion caused by the obstacle.

EXPERIMENTAL REALIZATION

Three situations are compared to verify the cloaking performance of the ultrathin cloak: the bare case without obstacle and cloak (Figure 3A), the obstacle-only case with obstacle but no cloak (Figure 3B), and the cloak case with both obstacle and cloak (Figure 3C). For the bare case, streamlines remain parallel and uniform in all regions, since there is no disturbance at all. For the obstacle-only case, the streamlines and the iso-pressure contours are significantly distorted and repelled by the obstacle. For the cloak case, however, the streamlines and the iso-pressure contour out of the cloaking shell become parallel again, as if the cloaked obstacle is absent. Beyond these simple simulations of assuming uniform permeability in each region in Figures 3A–3C, we further numerically construct the porous medium and obtain similar simulation results in Figures 3D–3F.

We then experimentally realize the ultrathin cloak in microfluidic devices. All the structural parameters of the three cases are scaled up twice for the sake of fabrication and flow visualization. The devices are fabricated by photolithography. First, a silicon wafer is coated by a layer of SU-8, an epoxy-based negative photoresist, and then covered by the chromium (Cr) photomasks with the pre-designed pattern. After UV light irradiation and development, the pattern is etched into the SU-8 layer. Then, liquid polydimethylsiloxane (PDMS) fills the SU-8 pattern and hardens into a solid. We peel off the PDMS and attach it to a glass slide, and the final microfluidic device is obtained (see Figure 3K). The dimensions of the microfluidic devices are 8 cm × 6 cm × 10μm.

We further perform experiments inside these three devices and measure the corresponding flow fields. Streamlines in each case are visualized by fluorescence microscopy. The working fluid is deionized water. Fluorescent particles, poly (methyl methacrylate) (PMMA) particles (density ρ = 1.03 g/cm^3) with the radius of 2μm dyed with rhodamine B, are dispersed in water as tracers (Stokes number $St \ll 1$) to visualize streamline of fluid flow. The volumetric concentration of fluorescent particles in water is 0.5 μL/mL, and the working fluid is injected steadily into the microfluidic device by a syringe pump. The imaging process is performed on the motorized microscope (Nikon TI-E), and the setup is shown in Figure 3J. Recordings are made with a scientific complementary metal-oxide-semiconductor (sCMOS) camera (Andor Zyla 4.2 PLUS USB 3.0; Andor Technology, Northern Ireland).

The snapshots of streamlines for the three cases are given in Figures 3G–3I. For the bare case with uniform pillars only, streamlines are parallel and uniform throughout the device (Figure 3G). When the obstacle is placed in the porous medium, streamlines are bent and disturbed around the obstacle (Figure 3H). However, once the obstacle is wrapped with the cloaking shell, the streamlines in the background become parallel and uniform again (Figure 3I), similar to the bare case without obstacle in Figure 3G (see Video S1 for more details). In addition, we have experimentally measured the velocity distribution in different positions along x in the case of with and without a cloak. All the experimental velocities are compared with the simulations of Figures 3D–3F, and the two datasets agree with each other well, as shown in Figure 3L.

Therefore, we have successfully realized an ultrathin cloak with a dimensionless thickness of 0.003, and in previous studies this value ranges from 0.02 to 1 or even larger. Our work thus sets a new record in the cloak thickness. Our hydrodynamic cloak in porous media could be useful in many applications. For example, cells and protein fibers are distributed in the environment of the human body and many locations can to some extent be regarded as liquid flow inside a porous medium. In some medical applications, we may want to put micro-devices inside the human body that make no disturbance to the body environment: our ultrathin cloak might find applications in these fields.

EXTENSION TO 3D AND DISCUSSIONS

Our 2D or cylindrical design can further be extended to a three-dimensional (3D) or spherical cloak. With a similar analysis, we can obtain the design parameter for permeability in 3D:

$$\frac{k_{\mathrm{II}}}{k_{\mathrm{III}}} = \frac{2R_2^3 + R_1^3}{2\left(R_2^3 - R_1^3\right)} \qquad \text{(Equation 9)}$$

Based on such design, we realize an ultrathin spherical cloak with thickness of 0.003 once again, as demonstrated in Figure 4. In the top row with the ultrathin cloak, the velocity and pressure fields are straight lines outside the object; however, in the bottom row without the cloak, these field lines are significantly distorted near the object. These simulation results clearly show that the ultrathin 3D cloak can be realized by putting a thin gap with a very small but proper thickness between the object and the porous background, the same as our previous 2D

results. Because the cloak is very small, the object with and without it looks very similar, as demonstrated in Figures 4C and 4F.

Moreover, our ultrathin cloak design can extend to another metamaterial design, concentrator, but not rotator. Because our ultrathin cloak design is based on the bilayer method instead of the transformation mapping theory, not all metamaterials designed by transformation mapping[16,30,31] can be realized by our method. In particular, a rotator requires anisotropic parameters coming from the coordinate transformation, which cannot be realized by our ultrathin method. However, a concentrator can be designed with the bilayer method[32] and thus is suitable for our ultrathin technique. Therefore, both ultrathin cloak and concentrator in a porous medium can be fabricated with our method.

Since the hydrodynamic cloak proposed previously is effective in drag reduction,[16] one may wonder whether the drag reduction is still valid for the ultrathin cloak. To demonstrate it, we calculate the drag forces with and without the ultrathin cloak, in a system with the same dimensions and conditions as our experiment. Our finite element analysis gives that, for the object without a cloak, the drag force is 2.2 mN, while it is 1.3 mN with a cloak. Thus, the drag force is reduced by 40% by our ultrathin cloak, which is not as good as the previous study.[16] However, considering the very thin thickness of our cloak, such a drag is already quite effective.

CONCLUSION

To summarize, inside a porous medium, we have designed and realized the thinnest shell-shaped cloak compared with all previous cloaks. Our cloak has a simple structure, consisting of only a thin shell of free space with designated thickness. The dimensionless thickness is only 0.003, which is about 10 times smaller than the previous ultrathin thermal cloak and three orders of magnitude smaller than the existing hydrodynamic cloaks. Although ultrathin, our cloak exhibits excellent cloaking performance in the actual flow field. This ultrathin hydrodynamics cloak may find potential applications in microfluidic devices or biomedical applications, and the free-space design also suggests a new and simple direction for cloak design.

REFERENCES

1. Pendry, J.B., Schurig, D., and Smith, D.R. (2006). Controlling electromagnetic fields. Science ***312***, 1780–1782.
2. Schurig, D., Mock, J.J., Justice, B.J., et al. (2006). Metamaterial electromagnetic cloak at microwave frequencies. Science ***314***, 977–980.
3. Leonhardt, U. (2006). Optical conformal mapping. Science ***312***, 1777–1780. https://doi.org/10.1126/science.1126493.
4. Shalaev, V.M. (2008). Physics. Transforming light. Science ***322***, 384–386.
5. Chen, H., Chan, C.T., and Sheng, P. (2010). Transformation optics and metamaterials. Nat. Mater. ***9***, 387–396.
6. Gömöry, F., Solovyov, M., Souc, J., et al. (2012). Experimental realization of a magnetic cloak. Science ***335***, 1466–1468.
7. Zhu, J., Jiang, W., Liu, Y., et al. (2015). Three-dimensional magnetic cloak working from dc to 250 kHz. Nat. Commun. ***6***, 8931.
8. Cummer, S.A., Popa, B.I., Schurig, D., et al. (2008). Scattering theory derivation of a 3D acoustic cloaking shell. Phys. Rev. Lett. ***100***, 024301.
9. Zhang, S., Xia, C., and Fang, N. (2011). Broadband acoustic cloak for ultrasound waves. Phys. Rev. Lett. ***106***, 024301.
10. Narayana, S., and Sato, Y. (2012). Heat flux manipulation with engineered thermal materials. Phys. Rev. Lett. ***108***, 214303.
11. Han, T., Bai, X., Gao, D., et al. (2014). Experimental demonstration of a bilayer thermal cloak. Phys. Rev. Lett. ***112***, 054302.
12. Li, Y., Li, W., Han, T., et al. (2021). Transforming heat transfer with thermal metamaterials and devices. Nat. Rev. Mater. ***6***, 488–507.
13. Fridman, M., Farsi, A., Okawachi, Y., and Gaeta, A. (2012). Demonstration of temporal cloaking. Nature ***481***, 62.
14. Zhou, F., Yan, S., Zhou, H., et al. (2019). Field-programmable silicon temporal cloak. Nat. Commun. ***10***, 2726–2728.
15. Tay, F., Zhang, Y., Xu, H., et al. (2019). A metamaterial-free fluid-flow cloak. Preprint at arXiv. https://doi.org/10.48550/arXiv.1908.07169.
16. Park, J., Youn, J.R., and Song, Y.S. (2019). Hydrodynamic metamaterial cloak for drag-free flow. Phys. Rev. Lett. ***123***, 074502.
17. Boyko, E., Bacheva, V., Eigenbrod, M., et al. (2021). Microscale hydrodynamic cloaking and shielding via electro-osmosis. Phys. Rev. Lett. ***126***, 184502.
18. Wang, B., Shih, T.M., Xu, L., et al. (2021). Intangible hydrodynamic cloaks for convective flows. Phys. Rev. Appl. ***15***, 034014.
19. Park, J., and Song, Y.S. (2020). Laminar flow manipulators. Extreme Mech. Lett. ***40***, 100908.
20. Wang, B., Shih, T.M., and Huang, J. (2021). Transformation heat transfer and thermo-hydrodynamic cloaks for creeping flows: Manipulating heat fluxes and fluid flows simultaneously. Appl. Therm. Eng. ***190***, 116726.
21. Narayana, S., and Sato, Y. (2012). DC magnetic cloak. Adv. Mater. ***24***, 71–74.
22. Zhan, J., Li, K., Zhou, Y., et al. (2021). Ultrathin conformal magnetic invisible cloak for irregular objects. ACS Appl. Mater. Interfaces ***13***, 17104–17109.
23. Xiang Jiang, W., Yang Luo, C., Lei Mei, Z., and Jun Cui, T. (2013). An ultrathin but nearly perfect direct current electric cloak. Appl. Phys. Lett. ***102***, 014102.
24. Xu, H., Shi, X., Gao, F., et al. (2014). Ultrathin three-dimensional thermal cloak. Phys. Rev. Lett. ***112***, 054301.
25. Han, T., Ye, H., Luo, Y., et al. (2014). Manipulating DC currents with bilayer bulk natural materials. Adv. Mater. ***26***, 3478–3483.
26. Xu, L., Dai, G., Wang, G., and Huang, J. (2020). Geometric phase and bilayer cloak in macroscopic particle-diffusion systems. Phys. Rev. E ***102***, 032140.
27. Urzhumov, Y.A., and Smith, D.R. (2011). Fluid flow control with transformation media. Phys. Rev. Lett. ***107***, 074501.
28. Masliyah, J.H., Neale, G., Malysa, K., and G.M. Van De Ven, T. (1987). Creeping flow over a composite sphere: solid core with porous shell. Chem. Eng. Sci. ***42***, 245–253.
29. Schulz, R., Ray, N., Zech, S., et al. (2019). Beyond Kozeny Carman: predicting the permeability in porous media. Transport Porous Media ***130***, 487–512.
30. Park, J., Youn, J.R., and Song, Y.S. (2021). Metamaterial hydrodynamic flow concentrator. Extreme Mech. Lett. ***42***, 101061.
31. Park, J., Youn, J.R., and Song, Y.S. (2019). Fluid-flow rotator based on hydrodynamic metamaterial. Phys. Rev. Appl. ***12***, 061002.
32. Shen, X., Li, Y., Jiang, C., et al. (2016). Thermal cloak-concentrator. Appl. Phys. Lett. ***109***, 031907.

ACKNOWLEDGMENTS

We thank for Prof. Yilin Wu for providing the experimental setup for fluid visualization. L.X. acknowledges the financial support from GRF-14307721, NSFC-12074325, Guangdong Basic and Applied Basic Research Fund 2019A1515011171, GRF-14306518, CRF-C6016-20G, CRF-C1006-20WF, TK1914385, and RMGS Matching grant CUHK8601417. X.S. acknowledges the financial support from Guangdong Basic and Applied Basic Research Foundation 2019A1515110211.

AUTHOR CONTRIBUTIONS

M.C. performed simulations, experiments, and data analysis, and prepared the manuscript. X.S. and M.C. discussed the theoretical explanation. X.S. and L.X. revised the manuscript. L.X. supervised the research.

DECLARATION OF INTERESTS

The authors declare no competing interests.

SUPPLEMENTAL INFORMATION

Supplemental information can be found online at https://doi.org/10.1016/j.xinn.2022.100263.

LEAD CONTACT WEBSITE

http://www.phy.cuhk.edu.hk/∼xulei/homepage/.